

# Signature of Tonga Volcanic Eruption in the ionosphere over South America

Hisao Takahashi<sup>1</sup>, Cosme Alexandre O. B. Figueiredo<sup>1</sup>, Diego Barros<sup>2</sup>, Cristiano M. Wrasse<sup>1</sup>, Gabriel Augusto Giongo<sup>3</sup>, Rogerio H. Honda<sup>1</sup>, Luiz F. R. Vital<sup>1</sup>, Laysa Cristina Araujo Resende<sup>4</sup>, Prosper Kwamla Nyassor<sup>5</sup>, Toyese Tunde Ayorinde<sup>1</sup>, Carolina S Calmo<sup>1</sup>, Marcelo Banik de Padua<sup>5</sup>, and Yuichi Otsuka<sup>6</sup>

<sup>1</sup>Instituto Nacional de Pesquisas Espaciais

<sup>2</sup>Unknown

<sup>3</sup>Southern Regional Space Research Center

<sup>4</sup>National Institute for Space Research/China-Brazil Joint Laboratory of Space Weather

<sup>5</sup>National Institute for Space Research

<sup>6</sup>Nagoya University

November 25, 2022

## Abstract

On January 15, 2022, we observed various unusual atmospheric wave events over the South American sector: Atmospheric pressure waves (Lamb mode) around 12:30 to 17:30 UT, Tsunamis along the Chile coast at around 17:00 to 19:00 UT, and related ionospheric disturbances between 11:30 and 20:00 UT. We understand that these events were generated by the Tonga volcanic eruption that occurred at (20.55°S, 175.39°W) in South Pacific Ocean at 04:15 UT. Several Traveling Ionospheric Disturbances (TIDs) were observed before and after the Lamb wave passed over the continent and the arrival of the tsunami on the Chile coast. This is the first time to report the signature of ionospheric disturbances over the South American continent generated by both the Lamb wave and the tsunami that were produced by the huge volcanic eruption.

## Hosted file

essoar.10511884.1.docx available at <https://authorea.com/users/540949/articles/605333-signature-of-tonga-volcanic-eruption-in-the-ionosphere-over-south-america>

## Hosted file

agu\_supinfo\_takahashi.docx available at <https://authorea.com/users/540949/articles/605333-signature-of-tonga-volcanic-eruption-in-the-ionosphere-over-south-america>

## Signature of Tonga Volcanic Eruption in the ionosphere over South America

H. Takahashi<sup>1</sup>, C. A. O. B. Figueiredo<sup>1</sup>, D. Barros<sup>1</sup>, C. M. Wrasse<sup>1</sup>, G. A. Giongo<sup>1</sup>, R. H. Honda<sup>1</sup>, L. F. R. Vital<sup>1</sup>, L. C. A. Resende<sup>1,2</sup>, P. K. Nyassor<sup>1</sup>, T. T. Ayorinde<sup>1</sup>, C. S. Carmo<sup>1</sup>, M. B. Padua<sup>1</sup>, Y. Otsuka<sup>3</sup>.

<sup>1</sup>Instituto Nacional de Pesquisas Espaciais, São José dos Campos, Brazil

<sup>2</sup>State Key Laboratory of Space Weather, Beijing, China

<sup>3</sup>Institute for Space-Earth Environmental Research, Nagoya University, Nagoya, Japan

Corresponding author: Hisao Takahashi (hisao.takahashi@inpe.br)

### Key Points:

- We observed traveling ionospheric disturbances over the south America after the Tonga volcanic eruption occurred on 15 January 2022.
- The TIDs appeared before and after the arrivals of the atmospheric pressure Lamb wave and the ocean tsunami.
- The observational evidence of TIDs, Lamb wave and the tsunami is the first time to report from the South American continent.

### Abstract

On January 15, 2022, we observed various unusual atmospheric wave events over the South American sector: Atmospheric pressure waves (Lamb mode) around 12:30 to 17:30 UT, Tsunamis along the Chile coast at around 17:00 to 19:00 UT, and related ionospheric disturbances between 11:30 and 20:00 UT. We understand that these events were generated by the Tonga volcanic eruption that occurred at (20.55°S, 175.39°W) in South Pacific Ocean at 04:15 UT. Several Traveling Ionospheric Disturbances (TIDs) were observed before and after the Lamb wave passed over the continent and the arrival of the tsunami on the Chile coast. This is the first time to report the signature of ionospheric disturbances over the South American continent generated by both the Lamb wave and the tsunami that were produced by the huge volcanic eruption.

### Plain Language Summary

A huge volcanic eruption occurred at the volcano Hunga Tonga-Hunga Ha'apai (20.55°S, 175.39°W), one of the islands of the Tonga archipelago in the South Pacific Ocean, on 15 January 2022, at 04:15 UT (Universal Time). The eruption provoked earthquake and tsunami on the earth surface and released a huge amount of thermal energy and volcanic ashes into the atmosphere that reached up to ~50 km altitude. Such an explosive release of thermal energy produced atmospheric pressure waves, acoustic waves, and internal gravity waves in the lower atmosphere propagating horizontally and vertically up to the ionosphere (above 200 km altitude). The present work, as the first time, reports signatures

of the ionospheric disturbances caused by the tsunami and atmospheric pressure waves over the South American continent.

## 1 Introduction

On 15 January 2022 at 04:15 UT a large under-water volcanic eruption occurred at Hunga Tonga Hunga Ha’apai (20.55°S, 175.39°W) in the archipelago of Tonga (hereafter Tonga eruption), South Pacific Ocean. NOAA (National Oceanic and Atmospheric Administration), USA, informed that the gas released explosively reached 40 km altitude, and the atmospheric pressure wave left from the center of eruption expanded radially as a mode of Lamb wave [Duncombe, 2022]. Subsequently a variety of acoustic and gravity waves propagated to the upper atmosphere and ionosphere [Wright et al., 2022, Themens et al., 2022, Zhang et al., 2022]. Tsunamis were also generated and propagated on the Pacific Ocean ([https://irides.tohoku.ac.jp/research/prompt\\_investigation/2022\\_tonga-vol-tsunami.html](https://irides.tohoku.ac.jp/research/prompt_investigation/2022_tonga-vol-tsunami.html)).

Ionospheric disturbances during significant atmospheric events such as Earthquakes, tsunamis and volcanic eruptions have been occasionally studied. Especially the recent Tohoku earthquake on 11 March 2011 provoked a large amplitude of Tsunami, and subsequent ionospheric disturbances were observed by several research groups [Tsugawa et al [2011], Makela et al. [2011], Smith et al. [2015], Azeem et al. [2017]. In the case of volcanic eruptions, the earth’s atmosphere further affects different kind of disturbances. The explosive release of high temperature volcanic gas into the troposphere produces atmospheric pressure waves. It propagates radially between the ground surface and the troposphere without losing the wave energy as the Lamb mode [Lindzen and Blake, 1972]. Lamb wave propagates non-dispersive mode with a speed of sound  $\sim 310$  m/s. Although the propagation is confined in the troposphere, a part of wave energy releases to the mesosphere and the lower thermosphere [Nishida et al., 2014]. In the Tonga eruption, Wrights et al. [2022] showed a concentric Lamb wave from the Tonga Eruption area. The concentric wave structure of the temperature field in the stratosphere was observed by Atmospheric Infrared Sounder (AIRS) mounted on the Aqua satellite [Adam, 2022].

Ionospheric disturbances caused by the last Tonga eruption were quickly reported by Zhang et al., [2022] and Lin et al., [2022]. Themens et al. [2022], using GNSS ground receiver data, identified the large scale Traveling Ionospheric Disturbances (LSTIDs), horizontal wavelength longer than 1000 km near the Tonga eruption area, and Medium Scale TID (MSTIDs), horizontal wavelength between 350-950 km away from the eruption region. Lin et al. [2022] showed concentric TIDs driven by the Tonga eruption in geomagnetically conjugate points, Australia, and Japan. The global scale ionospheric disturbances, nowadays, can be monitored by the Global Navigation Satellite System (GNSS) and ground-based GNSS receiver systems. The present work aims to report the ionospheric disturbances during and after the Tonga eruption observed by the GNSS receiver network in the South American sector. The passage of Lamb waves over the continent and the arrival of the Tsunami on the coast of Chile

side, and the subsequent ionospheric disturbances are presented.

## 2 Observations

In the present work, we observed the atmospheric pressure variation by the barometer data, sea level variation by the Tsunami sensor buoy data, and the ionospheric disturbance by the ground-based GNSS receiver data. Measurements of the ground-level atmospheric pressure have been carried out by world-wide GNSS ground-based meteorological stations. The data collection frequency is 1/min. The data from the Brazilian side are available in the RBMC (Rede Brasileiro de Monitoramento Contínuo) of IBGE (Instituto Brasileiro de Geografia e Estatística) at the site: <https://www.ibge.gov.br/geociencias/informacoes-sobre-posicionamento-geodesico/rede-geodesica/16258-rede-brasileira-de-monitoramento-continuado-dos-sistemas-gnss-rbmc.html?=&t=o-que-e>.

The data from the Chilean meteorological stations are available at, [\\*https://climatologia.meteochile.gob.cl/](https://climatologia.meteochile.gob.cl/).

Data of the ocean sea level are available at the site <http://www.ioc-sealevelmonitoring.org/index.php>, which is published by the Global Sea level Observing System (GLOSS/UNESCO). The data collecting frequency is 1/min. In the present work, we used 3 monitoring sites along the Chile coast ( $\sim 72^\circ\text{W}$ ) and one at Easter Island ( $27.2^\circ\text{S}$ ,  $109.4^\circ\text{W}$ ). The Tsunami arrival time and the amplitude of the sea level oscillation are used.

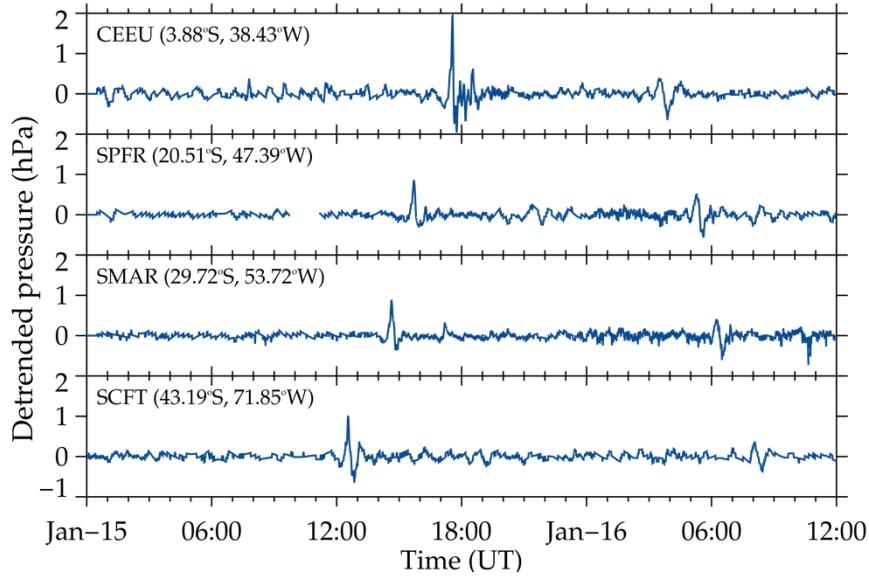
The Total Electron Content (TEC) is obtained from the GNSS receiver data, which are available on the site RBMC/IBGE. Ionospheric Total Electron Content (TEC) can be obtained by using a phase difference between the two carrier frequencies of the GNSS satellite. One TEC unit corresponds to  $10^{16}$  electrons/ $\text{m}^2$  column. Normally, the amplitude of disturbance of TEC in the ionosphere by the Travelling Ionospheric Disturbances (TIDs) is less than one TEC unit [Otsuka et al., 2013]. In order to detect such a small amplitude of variation, we used detrended TEC. According to Otsuka et al. [2013], the detrended TEC was obtained from subtracting 1-hour running average from the slant TEC including the inter-frequency biases. Then, the slant component was converted to vertical one. The procedure of TEC and dTEC calculations have been reported elsewhere. [Otsuka et al, 2013, Figueiredo et al., 2018].

## 3 Results

### 3.1 Atmospheric pressure (Lamb) wave

The Lamb wave reached the south coast of Chile at Futaleufu: SCFT( $71.9^\circ\text{W}$ ,  $43.2^\circ\text{S}$ ) at 12:29 UT with an amplitude of  $\pm 1.0$  hPa. Figure 1(a) shows temporal variations of the ground level atmospheric pressure measured at 4 observation sites from Chile to Brazil on 15 January 2022. After the arrival of the Lamb wave at SCFT on 12:29 UT, it arrived at Santa Maria: SMAR ( $53.7^\circ\text{W}$ ,  $29.7^\circ\text{S}$ ) on 14:38 UT, Franca: SPFR( $47.4^\circ\text{W}$ ,  $20.5^\circ\text{S}$ ) at 15:38 UT, and Fortaleza: CEEU ( $38.4^\circ\text{W}$ ,  $3.9^\circ\text{S}$ ) in the low latitude region on 17:29 UT. The Lamb wave took around 5.0 hours to cross the South American continent from the SW to NE.

Also, can be recognized is that there are return waves from 03:00 to 08:00 UT on 16 January 2022 as can be seen in Figure 1. These observational events suggest that the Lamb wave started from the Tonga eruption, propagating as a concentric form, bouncing at the antipodal point in North Africa, and generating a return wave. The phase velocity and propagation direction of the Lamb wave over the South American continent were obtained from the time delay between the observation sites. In this calculation we used 30 ground-based GNSS meteorological sites that have an atmospheric pressure sensor (barometer). Figure 1(b) shows the relation between longitudinal (latitudinal) distances measured from a reference point at (45.92°S, 71.68°W) and the time delay of the peak occurrence of the observation sites. The phase speed obtained from the linear relation of the plots is  $304.5 \pm 5.6$  m/s, which is slower than that was observed near the South Pacific region, 318 m/s (Wright et al., 2022). The azimuth of the direction of propagation was  $46.7^\circ$ (NE).



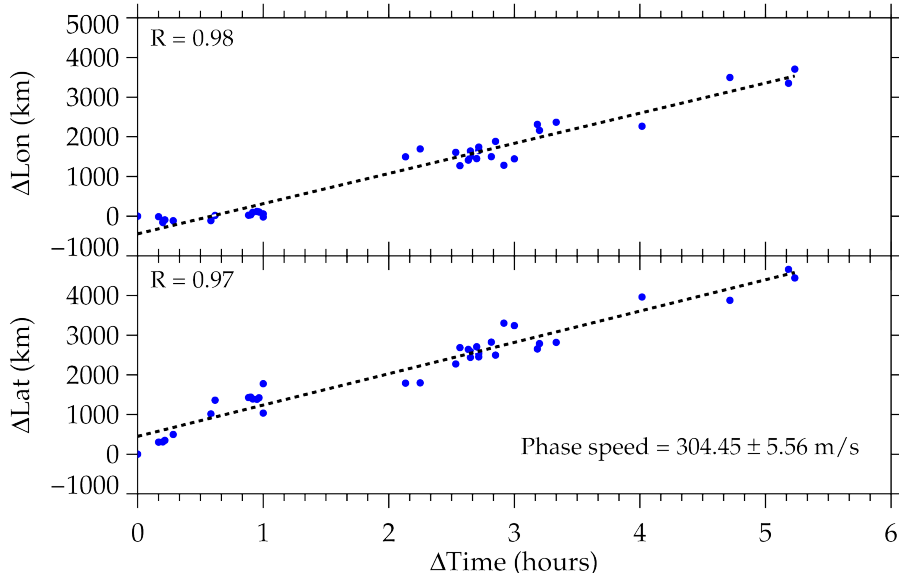


Fig. 1. Atmospheric pressure observation over South America: (upper panel) Occurrence of the Lamb wave at 4 locations, (lower panel) Longitudinal (top) and latitudinal (down) time delays between the 30 observation sites over the South America (Chile and Brazil).

### 3.2 Tsunami

The arrival of the tsunami on the southern coast of Chile is shown in Figure 2. It shows a temporal variation of sea surface measured by buoy as mentioned in the previous section. A high-pass filter with a 120 min window was applied to take longer period (tidal) oscillations out. It is clear to identify the arrival of the tsunami wave at Easter island (27.2°S, 109.4°W,) at 13:50 UT. On the Chilean coast, it arrived at Bahia Mansa (40.6°S, 73.7°W) at 17:15 UT, followed by Valparaiso (33.0°S, 71.6°W) and Tocopilla (22.1°S, 70.2°W) at around 18:00 UT. One can notice that the tsunami wave first arrived at the south of the Chilean coast and then went to the middle to low latitude region. The period of oscillation of the sea surface is somewhat short around 12 min (at Easter). At Bahia Mansa, the period is long, 20 to 30 min in the beginning at around 17:00 UT, then became shorter (11 min). The amplitude of oscillation (peak to peak) was 46 cm at Easter, 100 cm at Bahia Mansa, and 20 to 50 cm at Valparaiso to Tocopilla in the middle to low latitudes. The amplitude of oscillation is dependent on the landscape of the coast, too. Global scale simulation of the tsunami waves ([https://irides.tohoku.ac.jp/research/prompt\\_investigation/2022\\_tonga-vol-tsunami.html](https://irides.tohoku.ac.jp/research/prompt_investigation/2022_tonga-vol-tsunami.html)) showed the first arrival of the tsunami on the southern coast of Chile.

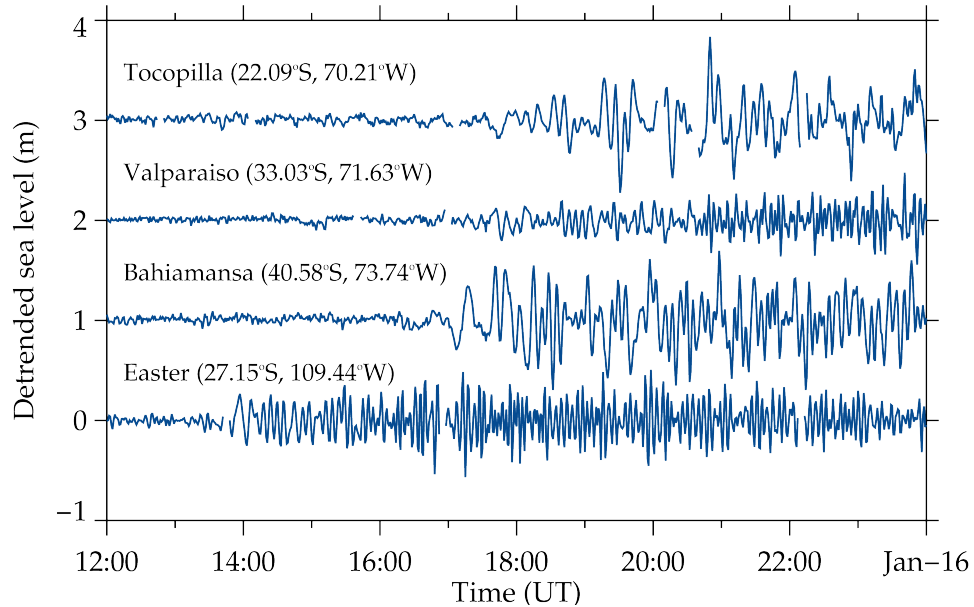


Fig. 2. Tsunami induced sea surface oscillation observed at Easter, Bahiamansa, Valparaiso and Tocopilla at the Chile coast. The red arrow indicates the first arrival of tsunami.

### 3.3 Ionospheric TEC map

Figure 3 shows detrended TEC (dTEC) maps over South America. The dTEC map at 12:35 UT (Figure 3(a)) shows a wavefront in the south of Chile to Argentine ( $40^{\circ}\text{S}$ ,  $75^{\circ}\text{W}$ ), highlighted by a blue circle in the figure. The wavefront is aligned NW to SE moving toward NE. At around 17:30 UT another wave structure started from the south. The waves are similar to the previous one but with several wavefronts propagating toward NE. Figure 3(b) is a snapshot of the wave structure at 18:36 UT. One can notice that there are longitudinally extended long waves in the region of ( $30^{\circ}\text{S}$ ,  $65^{\circ}\text{W}$ ) and a short form of wave structure at around ( $35^{\circ}\text{S}$ ,  $70^{\circ}\text{W}$ ), those highlighted by a blue circle in the figure. Figure 3(c) shows the wave packet propagating toward the low latitudes at 19:38 UT. The movement of the wave packets is presented in a **supporting information file, S1**.

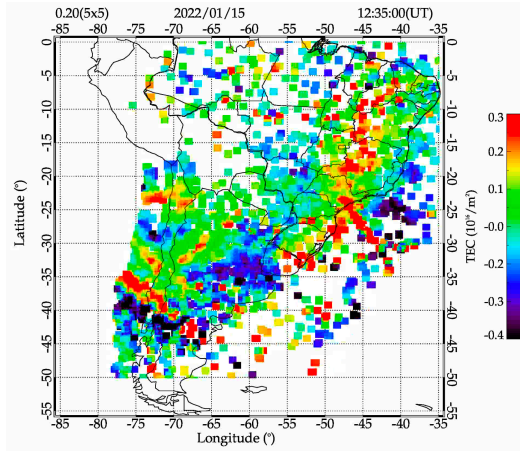


Fig. 3. Ionospheric dTEC map over South America on 15 Jan 2022, (a) TID starting from the Chile side at 12:35 UT, (b) TIDs in the highlighted circle at 18:36 UT, (c) TIDs from the Argentine to Brazil side at 19:38 UT. The color bar shows the amplitude of dTEC oscillation (0.3 to -0.4 TECu). The blue circles highlight the region of TIDs.

To retrieve characteristics of the observed waves, longitudinally (latitudinally) sliced images at a fixed latitude (longitude) are plotted as a function of time in UT (keogram). Figure 4 presents the keogram with the longitudinal cut (55-80°W) at a fixed latitude 35°S (upper panel) and the latitudinal cut (20-50°S) at a fixed longitude 70°W (lower panel) as a function of UT. From the figure, one can notice that there are two time zones, one at 11:30 – 14:00 UT and the other at 16:00 – 20:00 UT, when several waves are propagating toward NE and SE. They occurred before and immediately after the arrival of the Lamb wave at 12:30 UT and the tsunami at 17:15 UT. It should be noted that the wave packets before and after the Lamb wave are narrow, having only one to two wave crests. On the other hand, the wave packets around the arrival of the tsunami have several wave crests extending for more than 4 hours. Similar keogram analysis was also applied for the Brazilian side (not shown here) to find out the wave packets.

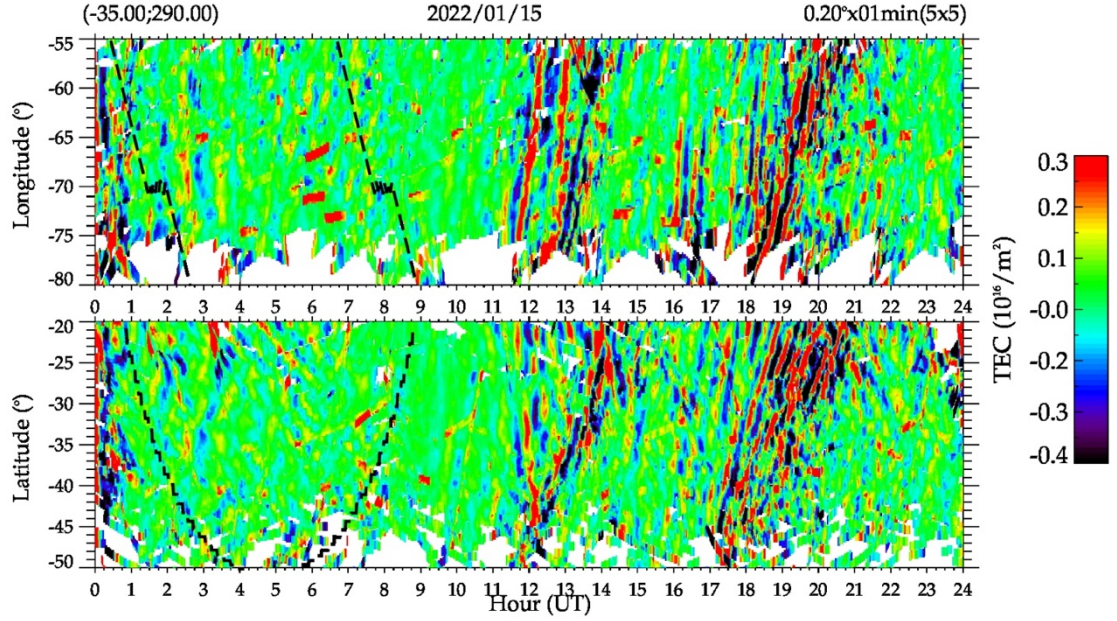


Fig. 4. Keogram of the dTEC maps of the Chile side: longitudinal cut at 35°S (upper panel) and latitudinal cut at 70°W (lower panel) as a function of time (UT) on 15 Jan 2022. The color bar shows the amplitude of dTEC oscillation. The black lines indicate arrival of the Lamb wave at 12:30 UT and the tsunami at 17:15 UT at Chile coast around 40°S. The broken and dashed lines indicate sunset and sunrise time in the ionosphere at 300 km altitude.

#### 4 Discussion

On 15 January 2022, we observed the atmospheric pressure wave (Lamb mode), tsunami, and ionospheric TIDs in the South American continent, which must be related to the Tonga volcanic eruption. As can be seen in the dTEC keograms in Figure 4, there are two groups of TID activities, one at the 12:00 to 14:00 UT, and the other at the 16:00 to 20:00 UT time zones. The horizontal wavelengths, periods, phase speed, propagation direction, and amplitude of oscillations were calculated from the sequence of the dTEC maps to investigate the characteristics of these wave propagation properties. The wave characteristics are summarized in Table 1, together with the Lamb wave and the tsunami characteristics.

**Table 1.** Wave characteristics of Lamb wave, tsunami and 9 TIDs observed at Chile side (35°S, 70°W) and Brazilian side (23°S, 53°W) during 11:30 and 20:00 UT on 15 January 2022. (SCFT: Futaleufu/Chile, BHM: Barra Mansa/Chile)

Waves	Location (Lat, Lon) (deg)	Reach & Start time (UT)	Horizontal wavelength (km)	Period
<b>Lamb wave</b>	SCFT(43.2S, 71.9W)	<b>12:30</b>	--	<b>solitar</b>
<b>Tsunami</b>	BHM(40.6S, 73.7W)	<b>17:15</b>	--	<b>32, 26</b>
<b>TID-1</b>	30-40S (Chile)	11:30	1,174 ±117	36±1

Waves	Location (Lat, Lon) (deg)	Reach & Start time (UT)	Horizontal wavelength (km)	Period
<b>TID-2</b>	30-40S (Chile)	11:45	946±95	36±2
<b>TID-3</b>	40- 45S (Chile)	<b>12:30</b>	<b>479±88</b>	<b>20±5</b>
<b>TID-4</b>	35-40S (chile)	<b>13:15</b>	<b>348±6</b>	<b>19.7±</b>
<b>TID-5</b>	30-40S (Chile)	16:05	875±41	31±01
<b>TID-6</b>	40-45S (Chile)	<b>17:30</b>	<b>505±70</b>	<b>24±5</b>
<b>TID-7</b>	35-40S (Chile)	<b>18:35</b>	<b>330±9</b>	<b>20±0.</b>
TID-8	20-30S (Brazil)	15:31	366±40	20±2
TID-9	20-30S (Brazil)	19:00	667±60	28±3

In the Chile side (30- 45°S, 70°W), in total 7 TIDs were identified, i.e., two TIDs (11:30, 11:45 UT) before the arrival of Lamb wave (12:30 UT), two TIDs (12:30, 13:15 UT) after the arrival of the Lamb wave, one (16:05 UT) prior to the arrival of the tsunami, and two (17:30, 18:35 UT) after the arrival of the tsunami. On the Brazilian side (20-30°S, 50°W), two TIDs were identified, one (15:31 UT) related to the Lamb wave passage and the other (19:00 UT) probably related to the tsunami. These 9 TIDs have the horizontal wavelength of 330 to 1174 km, the period of 20 to 36 min, and the phase speed of 275 to 544 m/s. Their propagation directions are 20° to 40° (NE), except one toward 139° (SE). These TIDS can be recognized in the keograms (Figure 4), too.

**Two groups of TIDs related to Lamb wave and Tsunami:** Special attention should be taken for the TID-3 at 12:30 and TID-6 at 17:30. The two waves appeared almost simultaneously with the arrival of the Lamb wave (12:30 UT) and the tsunami (17:15 UT), respectively. Subsequent waves, TID-4 (13:15) and TID-7 (18:35), can be seen as the continuation of the first ones but with shorter wavelengths. As can be seen in the keograms (Figure 4), the first group might be generated by the Lamb wave and the second group by the tsunami. Regarding the fact of no time difference between the ionospheric disturbance and the tsunami, Smith et al. [2015] reported that there was no measurable time difference between the tsunami arrival and the TID event observed at El Leoncito (Andes Mountains) in the case of the Tohoku Earthquake event in 2011. How these TID waves in the ionosphere did appear without time lag against the tsunami should be further investigated. As far as we understand it is the first time to observe TIDs related to both Lamb wave and the tsunami, almost simultaneously.

**TIDs prior to the arrival of Lamb wave and Tsunami:** It is interesting to point out that there are two waves before the arrival of the Lamb wave, TID-1 (11:30) and TID-2 (11:45). They have longer wavelengths (1174 and 946 km) and faster (544 and 438 m/s), one propagating SE and the other propagating NE. By considering the wave characteristics, different from the TID-3 and TID-4, we suppose that they were generated far away from the Chile coast and propagated to the direction of the South American side with a faster phase speed than the Lamb wave. A similar characteristic can be seen in TID-5, which appeared one

hour earlier (16:05 UT) than the arrival of the tsunami (17:15 UT), having a long wavelength (875 km) and a fast speed (470 m/s). Makela et al. [2011] observed the ionospheric wave structure by OI 630 nm airglow imager at Hawaii islands after the Tohoku Earthquake on 11 March 2011, that proceeded the ocean tsunami by approximately one hour. Azeem et al. [2017], on the other hand, reported that the TID event over the North America occurred after the arrival of the tsunami on the coast of California. The two different observation results might be related to the different generation processes. From the GW simulation model, Vadas et al. (2015) derived the atmospheric acoustic waves and GWs excited by an ocean surface wave packet with a specific frequency and duration. The authors concluded that if an ocean wave packet has a sum period longer than 10–12 min, then the excited GWs could have much faster horizontal phase speeds than that of the ocean wave, and thus reach a fixed location well before the ocean wave packet. Our present results, TIDs before the arrival of the tsunami, could be explained by this model. Further simulation model would need for the case of the Lamb wave.

***TIDs in the Brazilian longitude:*** We could identify two TIDs over the Brazilian sector ( $\sim 50^\circ\text{W}$ ), one TID-8 at 15:31 UT and the other TID-9 at 19:00 UT. The former corresponds to the arrival of the Lamb wave over Brazil and the latter corresponds to the arrival of TIDs generated on the Chile side (see Supporting file S1). It should be noted that during the passage of the Lamb wave at SMAR at 14:38 UT (see Fig. 1), at SPFR at 15:43 UT and at CEEU at 17:34 UT, the TID wavefronts were observed almost simultaneously. It indicates that the Lamb wave might provoke perturbation in the ionosphere almost in time. Lin et al, [2022] discussed that the gravity waves generated by the Lamb wave travel with the same speed, locked to the propagation of Lamb mode. Our present results also did show a close relation between the Lamb wave and ionospheric TIDs. Further observations and simulations are, however, needed to investigate how Lamb waves could propagate into the upper atmosphere and ionosphere so rapidly.

***Comparison of TID-3 (12:30) and TID-6 (17:30):*** Although the wave sources of the TID-3 and TID-6 seem to be different, their wave characteristics have no difference. The horizontal wavelengths of 480-505 km, period of 20-24 min and phase speed of 350-400 m/s, propagating toward  $20\text{-}30^\circ\text{N}$ . The amplitude of oscillation is, however, a little different, the TID-3 has 0.6 TECu, compared to the TID-6 with 0.3 TECu. The spatial scale of the wave packet is also different. The TID-3 has only one to two wavefronts, against the TID-6 having several wavefronts (3 to 4). This difference might be due to the source of gravity waves. The Lamb wave is a solitary wave. On the other hand, the tsunami produced several periodic oscillations generating atmospheric gravity waves along the coast of Chile.

***Effect of Geomagnetic activity:*** From the evening of 14 to the early morning of 15 January 2022, a moderate geomagnetic activity ( $K_p \sim 4\text{-}5$ ) was going on. The main phase ( $\text{Dst} \sim -90$  nT) was around 23:00 UT on 14 January 2022. It was in

a recovery phase when the Tonga eruption occurred. During the time zone of 11:00 to 20:00 UT, the Kp index varied from 4 to 2, the Dst index varied from -55 to -17 nT. The auroral activity (AE index) varied less than 500 nT, except in the time zone of 13:30-14:00 UT when it was larger than 500 nT. Looking into the keogram of dTEC (Figure 4), there are some dTEC disturbances in the period of 00:00 to 04:00 UT, which might be related to the geomagnetic activity. The TID-1 (11:30 UT), which is the longest (1174 km) and the fastest (544 m/s) wave in our present data is only one which has the different direction of propagation to SE. Although the AE index was moderate, a possibility of generation of LSTID by the auroral activity at around 11:00 UT could not be ruled out.

## 5 Conclusions

We observed a strong atmospheric pressure wave (Lamb mode), the tsunami, and 9 distinct TID wave packets in the ionosphere over South America from 11:00 to 20:00 UT on 15 January 2022, those must be related to the Tonga volcanic eruption in the South Pacific ocean occurred at 04:15 UT on the same day. Two groups of TIDs were observed, respectively, before and immediately after the Lamb wave and the tsunami arrival. The TID waves have the horizontal wavelength of 300-500 km, the period of 20-30 min, the phase speed of 270 – 400 m/s, and the propagation direction of 20°- 40° from the North. No significant time difference was observed between the TID-3 and the Lamb wave arrival, and TID-6 and the tsunami arrival. Exceptionally longer wavelengths (900-1200 km) and faster TIDs (470-540 m/s) were also observed prior to the Lamb wave and the tsunami arrivals. This observational evidence is the first time reported from the South American continent. Further simulation study would be necessary to understand the simultaneous occurrence of the Lamb wave in the troposphere and disturbances in the ionosphere.

## Data Availability

GNSS ground-based receiver data, used in the present study, are available from IBGE (Instituto Brasileiro de Geografia e Estatística) at <<https://www.ibge.gov.br/geociencias>>. The atmospheric pressure data in Chile are available from DGAC (Direção Meteorológica do Chile) at <<https://climatologia.meteochile.gob.cl/>>. The ocean sea level data are available from the Sea level observing system/UNESCO at the site: <<http://www.ioc-sealevelmonitoring.org/index.php>>.

## Acknowledgments

We thank the Brazilian Ministry of Science, Technology and Innovation (MCTI) and the Brazilian Space Agency (AEB) who supported the present work under the grants PO 20VB.0009. The present work was also supported by CNPq (Conselho Nacional de Pesquisa e Desenvolvimento) under the grants 310927/2020-0, 140401/2021-0, 163874/2021-2, 300322/2022-4, 150261/2022-5 , 300264/2022-4 ; Fundação de Amparo à Pesquisa do Estado de São Paulo (FAPESP) under the grants 2018/09066-8 and 2019/22548-4 ; and Coordenação de Aperfeiçoamento

de Pessoal de Nível Superior (CAPES) under the process 88887.514072/2020-00. Y. Otsuka was supported by JSPS KAKENHI Grant (20H00197, 21H04518), JSPS Bilateral Joint Research Projects (JPJSBP120226504), and JSPS Core-to-Core Program, B. Asia-Africa Science Platforms. L. C. A. Resende would like to thank the China-Brazil Joint Laboratory for Space Weather (CBJLSW), National Space Science Center (NSSC), Chinese Academy of Sciences (CAS) for supporting her postdoctoral.

## References

- Adam, D. (2022), Tonga Volcano Created Puzzling Atmospheric Ripples, *Nature*, 602, 3, 2022, doi:10.1038/d41586-022-00127-1.
- Azeem, I., S. L. Vadas, G. Crowley, and J. J. Makela (2017), Traveling ionospheric disturbances over the United States induced by gravity waves from the 2011 Tohoku tsunami and comparison with gravity wave dissipative theory, *J. Geophys. Res. Space Physics*, 122, doi:10.1002/2016JA023659.
- Duncombe, J. (2022), The surprising reach of Tonga's giant atmospheric waves, *Eos*, 103, <https://doi.org/10.1029/2022EO220050>.
- Figueiredo, C. A. O. B., Takahashi, H., Wrasse, C. M., Otsuka, Y., Shiokawa, K., & Barros, D. (2018). Medium-scale traveling ionospheric disturbances observed by detrended total electron content maps over Brazil. *Journal of Geophysical Research: Space Physics*, 123, 2215–2227. <https://doi.org/10.1002/2017JA025021>.
- Lin, J-T, Rajesh, P.K., Lin, C.C.H., Chou, M-Y, Liu, J. Y., Yue J., Hsiao, T.Y., Tsai, H-F, Chao, H-M, Kung, M-M. (2022), Rapid Conjugate Appearance of the Giant Ionospheric Lamb Wave in the Northern Hemisphere After Hunga-Tonga Volcano Eruptions. <http://www.essoar.org/doi/10.1002/essoar.10510440.1> (2022)
- Lindzen, R.S., Blake, D., 1972. Lamb waves in the presence of realistic distributions of temperature and dissipation, *J. geophys. Res.*, 77, 2166–2176. <https://doi.org/10.1029/JC077i012p02166>
- Makela, J. J., et al. (2011), Imaging and modeling the ionospheric airglow response over Hawaii to the tsunami generated by the Tohoku earthquake of 11 March 2011, *Geophys. Res. Lett.*, 38, L13305, doi:10.1029/2011GL047860.
- Nishida, K, Kobayashi, N., and Fukao, Y. (2014), Background Lamb waves in the Earth's atmosphere, *Geophys. J. Int.* (2014) 196, 312–316 doi: 10.1093/gji/ggt413.
- Otsuka, Y., K. Suzuki, S. Nakagawa, M. Nishioka, K. Shiokawa, and T. Tsugawa (2013), GPS observations of medium-scale traveling ionospheric disturbances over Europe, *Ann. Geophys.*, 31, 163–172, doi:10.5194/angeo-31-163-2013.

Smith, S. M., C. R. Martinis, J. Baumgardner, and M. Mendillo (2015), All-sky imaging of transglobal thermospheric gravity waves generated by the March 2011 Tohoku Earthquake, *J. Geophys. Res. Space Physics*, 120, 10,992–10,999, doi:10.1002/2015JA021638.

Themens, D. R., Watson, C., Žagar, N., Vasykveych, S., Elvidge, S., McCaffrey, A., et al. (2022). Global propagation of ionospheric disturbances associated with the 2022 Tonga volcanic eruption. *Geophysical Research Letters*, 49, e2022GL098158. <https://doi.org/10.1029/2022GL098158>

Tsugawa, T., A. Saito, Y. Otsuka, M. Nishioka, T. Maruyama, H. Kato, T. Nagatsuma, and K. T. Murata (2011), Ionospheric disturbances detected by GPS total electron content observation after the 2011 off the Pacific coast of Tohoku Earthquake, *Earth Planets Space*, 63, 875–879, doi:10.5047/eps.2011.06.035.

Vadas, S. L., J. J. Makela, M. J. Nicolls, and R. F. Milliff (2015), Excitation of gravity waves by ocean surface wave packets: Upward propagation and reconstruction of the thermospheric gravity wave field, *J. Geophys. Res. Space Physics*, 120, doi:10.1002/2015JA021430.

Wright, C.J., et al. (2022), Tonga eruption triggered waves propagating globally from surface to edge of space, *ESSOAr*, <https://doi.org/10.1002/essoar.10510674.1>

Zhang S-R, Vierinen J, Aa E, Goncharenko LP, Erickson PJ, Rideout W, Coster AJ and Spicher A (2022), 2022 Tonga Volcanic Eruption Induced Global Propagation of Ionospheric Disturbances via Lamb Waves. *Front. Astron. Space Sci.* 9:871275. doi: 10.3389/fspas.2022.871275.